Global biochemical analysis reveals miRNA-RNA virus and miRNA-enhancer targets regulating immune signalling in Respiratory syncytial virus infection

Sarah Ressel[1], Sujai Kumar[1], Jose Roberto Bermúdez-Barrientos[1], Katrina Gordon[1], Julia Lane[1], Jin Wu[2], Cei Abreu-Goodger[3], Jürgen Schwarze[4], Amy H. Buck[1,*]

[1] Institute of Immunology & Infection Research, School of Biological Sciences, University of Edinburgh, Edinburgh EH9 3FL, UK

[2] Janssen Research & Development, Janssen Pharmaceutica NV, Turnhoutseweg 30, 2340, Beerse, Belgium.

[3] Institute of Ecology and Evolution, School of Biological Sciences, University of Edinburgh, Edinburgh EH9 3FL, UK

[4] Child Life and Health, Centre for Inflammation Research, University of Edinburgh, Edinburgh EH16 4TJ, UK

*Corresponding author: a.buck@ed.ac.uk

Abstract

microRNAs (miRNAs) regulate nearly every physiological process but our understanding of exactly how they function remains incomplete, particularly in the context of viral infection. Target prediction models are built on canonical miRNA interactions with 3'untranslated regions (3'UTRs) and post-transcriptional gene suppression, leaving a gap in knowledge on other types of targets and capacity for direct interactions with viral genomes. Here we adapt a biochemical method to globally identify targets of human miRNAs in lung cells including scope for direct interactions with Respiratory syncytial virus (RSV). We show that RSV binds miR-26, miR-27, and let-7, leading to de-repression of miRNA targets associated with cell cycle regulation and immune signalling. Using our bioinformatics pipeline to determine high confidence targets in the human genome we further discover that pseudogenes which overlap transcriptional regulatory regions are functional miRNA targets. We identify and validate an interaction between miR-27 and a pseudogene-derived lncRNA that regulates transcription of *Carcinoembryonic antigen-related cell adhesion molecule 1* (*CEACAM1*). This work demonstrates that RSV directly interacts with host miRNAs to de-regulate host gene expression and provides biochemical support for the ability of miRNAs to directly regulate gene transcription linked to immune signalling.

Keywords:

miRNA, respiratory syncytial virus, regulation of gene expression, pseudogenes, lncRNA, regulatory RNA, CLEAR-CLIP

INTRODUCTION

Over the last two decades discoveries of direct RNA-RNA interactions between miRNAs and viruses have revealed non-canonical mechanisms for the regulation and function of miRNAs inside of cells. Some of the viral-miRNA interactions have been shown to increase genome stability, as first reported for the binding of miR-122 by hepatitis C virus (HCV) and more recently for miR-17 with *Pestivirus*es (1-4). Other viral-miRNA interactions inhibit the activity of the associated miRNA through sequestration from its host targets or by causing the miRNA to be degraded, as discovered in Herpesvirus saimiri (HVS) and murine cytomegalovirus (MCMV) which both use distinct viral transcripts to target miR-27 (5-8). While there is promise in blocking miRNA-virus interactions for therapeutic applications (9,10) these interactions cannot be reliably predicted.

The most reliable miRNA target prediction programs (such as TargetScan) only consider 3' untranslated regions (3'UTRs) of endogenous RNAs and are modelled based on assumptions of canonical repression and conservation (11). While these programs have enabled subsequent validation of high confidence 3'UTR targets, they cannot be applied to viral genomes and have created an implicit bias when studying miRNA functions. It has also been suggested that 3'UTR targeting is unlikely to explain all phenotypes associated with miRNA de-regulation (12,13). A more systematic understanding of the possible modes of action of miRNAs is therefore required to understand the consequences of miRNA de-regulation in viral infection and other disease. Since miRNAs are increasingly being used to control cell-specific expression of gene therapies (14), it is also timely to better define how miRNA perturbation or sequestration would affect different endogenous targets.

Biochemical approaches have become an important complement to computational methods for miRNA target identification. Various methods have been developed to identify miRNA-mRNA interactions by UV crosslinking and immunoprecipitation (CLIP) of AGO proteins followed by an intermolecular ligation step to generate chimeric sequences of miRNA and its target, including CLASH and CLEAR-CLIP (15-17). These methods have identified miRNA-target interactions in several viral families including *Flaviviridae* (4), however they have been refractory to the A549 cell line, a human lung cancer epithelial cell line that is routinely used to model gene regulation in the context of bacterial and respiratory virus infections as well as lung cancer, allergy, and asthma. Furthermore, very few published CLIP analyses examine non-canonical targets.

Here we first optimised the CLEAR-CLIP protocol (17) for the A549 cell line in order to build a comprehensive map of miRNA-target interactions in lung cells. We further developed a bioinformatic pipeline that maps the targets across the human and viral genomes, and accounts for interactions with elements beyond coding sequences (CDS) and 3'UTRs. We then compare A549 cells that are uninfected or those infected with Respiratory syncytial virus (RSV). RSV is a 15 kb negative-sense single-stranded RNA virus of the *Paramyxovirus* genus that has received a lot of attention recently due to surging cases after the corona virus pandemic. Despite the major clinical and economic burden in young children and the significant morbidity and mortality in the elderly caused by RSV, there is still no specific therapy and only limited active immunisation available (18). Several studies have proposed a role of viral proteins in causing miRNA de-regulation during infection (19-22). However, it is not known whether RSV directly interacts with or regulates miRNAs through RNA-RNA interactions.

Our global CLEAR-CLIP analysis shows that RSV interacts specifically with the miRNAs miR-26, miR-27, and let-7. We further demonstrate that many canonical miR-27 targets are de-repressed during infection including a large network of cell cycle genes. Through our genome analysis of high confidence miRNA-target reads we find that pseudogenes which overlap transcriptional regulatory regions are functional miRNA targets and we validate a specific interaction of miR-27 with a long noncoding RNA (lncRNA) that derives from a pseudogene which regulates the transcription of *Carcinoembryonic antigen-related cell adhesion molecule 1* (*CEACAM1).* This work identifies new mechanisms by which miRNA de-regulation can impact immune signalling and demonstrates that RSV directly modulates miRNA activity through RNA-RNA interactions.

MATERIALS AND METHODS

Cell lines and culture conditions

A549 human lung epithelial cells (CCL-185, ATCC) and human epithelial type 2 (HEp-2, CCL-23, ATCC) cells were cultured in Dulbecco's modified eagle medium (DMEM, Sigma-Aldrich) supplemented with 10% fetal bovine serum (FBS, Gibco), 1 % L-Glutamine (L-glut, Gibco) and 1 % Penicillin/ Streptomycin (P/S, Gibco) at 37 °C and 5 % CO_2. Cell lines were regularly checked for mycoplasma contamination by PCR with primers (forward: 5'-GGGAGCAAACAGGATTAGATACCC-3' and reverse: 5'-TGCACCATCTGTCACTCTGTTAACCTC-3').

Virus and infection conditions

The human RSV, strain A2, used in this study was provided by Janssen Pharmaceuticals (Belgium). To visualise progress of viral infection a modified virus was used that had the eGFP gene introduced into the viral genome as described in Hallak et al. (23) and Guerrero-Plata et al. (24). To determine viral titre, RSV immuno-plaque assays were performed in HEp-2 cells using 2-fold serial dilutions of the virus samples in DMEM. Cells were incubated with the virus dilution for 2 h before DMEM supplemented with 10 % FBS, 1 % L-glut, 1 % P/S was added, and the cells were incubated for further 22 h. The cells were then probed with 1:200 biotinylated RSV (Biorad) antibody and stained with 1:500 ExtrAvidin Peroxidase, with visualization of plaques by the addition of 3-Amino-9-EthylCarbazole (AEC) substrate. For infection assays in A549, the cells were seeded 24 h prior to infection and infected with RSV at a multiplicity of infection (MOI) of 0.1 in serum free DMEM (+1 % L-glut) for 1 h. Subsequently the cells were washed with serum free DMEM and incubated for a total of 48 h from the start of the infection in complete media (DMEM + 10 % FBS, 1 % L-glut) unless stated otherwise.

CLEAR-CLIP

The protocol described here was modified from the originally published CLEAR-CLIP(17) and modifications regarding buffers were guided by a variation of the protocol published by Bjerke and Yi (25). We further adapted the protocol to include a custom 3' adapter from TriLink (developed here) and adaptation to remove need for membrane transfer (developed here). The modified protocol is described below.

<u>Sample preparation</u>

A549 cells were grown in 245 mm square dishes. One day post-seeding cells were at about 80-90% confluency and either RSV-infected at an MOI of 0.1 or Mock-infected for 48 h. The plates were then washed with PBS and UV crosslinked (245 nm) on ice, covered with ice-cold PBS and UV irradiated at 200 mJ/cm^2 (or compared to 400 mJ/cm^2 or no crosslinking as detailed). The cells were harvested by scraping and immediately lysed in CLEAR-CLIP lysis buffer (50 mM Tris/HCl pH 7.5, 100 mM NaCl, 1 mM $MgCl_2$, 0.1 mM $CaCl_2$, 1 % Igepal, 0.5 % sodium deoxycholate, 0.1 % SDS, protease inhibitors (Roche)). After 10 min incubation on ice, lysates were DNase treated with 30 µL RQ1 RNase-free DNase and RNase treated with RNace-IT (Agilent) at a final concentration of 1:25,000 for 5 min at 37 °C with shaking. Lysates were cleared by centrifugation and 200 U RNasin RNase inhibitor (Promega) was added.

<u>Immunoprecipitation</u>

Protein G Dynabeads (Life Technologies) were prepared using 100 µL of beads coupled to 10 µg of AGO2 antibody (clone 11A9, Merck) or IgG control antibody (Rat IgG2a kappa Isotype Control (eBR2a), Invitrogen) per sample. Beads were equilibrated in lysis buffer before

the lysate was added to the beads and incubated rotating at 4 °C overnight. The beads were then washed as followed.

- 2x CLEAR-CLIP lysis buffer (1x the beads were directly resuspended in buffer, 1x 3 min rotation at 4 °C)
- 3x HS-CLEAR (50 mM Tris-HCl pH 7.4, 1 M NaCl, 1 mM EDTA, 1 % Igepal, 0.5 % sodium deoxycholate, 0.1 % SDS) for 3 min rotating at 4 °C each,
- 2x PNK+Tween (20 mM Tris-HCl pH 7.4, 10 mM $MgCl_2$, 0.2 % Tween-20)

All following reactions included 80 U RNase inhibitors and incubations were carried out with intermittent shaking.

5' phosphorylation, intermolecular ligation and 3' adapter ligation

The samples were then treated with 40 U of T4 polynucleotide kinase (PNK, 3' phosphatase minus, NEB) in a total reaction volume of 80 µL, including 10 mM ATP for 2.5 h at 20 °C to add a 5' phosphate group for the intermolecular ligation. Samples were subsequently washed 3x in PNK+Tween buffer. After the last wash, beads were flash centrifuged to remove residual buffer. The intermolecular RNA-RNA ligation was performed in a total volume of 100 µL using 62.5 U T4 RNA ligase 1 (NEB), 100 mM ATP, 15 % PEG-8000 at 16 °C overnight. The next day more ligase (25 U) and ATP (100 mM) were added to the reaction followed by further incubation for 5 h at 16 °C. The samples were washed 2x with CLEAR lysis buffer, followed by one wash in PNK/EDTA/EGTA buffer (50 mM Tris-HCl pH 7.4, 10 mM EDTA, 10 mM EGTA, 0.5 % Igepal) and two PNK+Tween washes. The samples were then treated with 8 U TSAP for 45 min at 20 °C and washed 2x in PNK+Tween buffer. A modified 3' sequencing adapter (3' CleanTag-IRDye800CW, TriLink, see Table S6, 1 µM) was ligated overnight at 16 °C in the dark using 800 U T4 RNA ligase 2 (truncated K227Q, NEB), 10 % PEG-8000 in a total reaction volume of 80 µL.

Elution from beads and SDS-PAGE purification of AGO2-RNA complexes

Beads were washed 2x with PNK+Tween and resuspended in elution buffer (15 µL 4x NuPAGE LDS sample buffer (Thermo Scientific), 45 µL PNK buffer (50 mM Tris-HCl pH 7.4, 50 mM NaCl, 10 mM MgCl2, 0.5 % TritonX-100, 5 mM β-Mercaptoethanol), 3 µL 1 M DTT). Samples were eluted from the beads at 70 °C with constant shaking. Eluate, containing AGO2-RNA complexes were run on a 4-12 % NuPAGE Bis-Tris protein gel for 150 min at 120 V in MOPS SDS running buffer (Thermo Scientific). Gels were run on ice to prevent RNA degradation and in the dark to protect the 3' adapter fluorophore. Fluorescent RNA was visualised using the Odyssey CLx scanner (Li-cor). The regions corresponding to 80-115 kDa or 115-185 kDa (see Table S1) were excised from the gel using a scalpel. Gel pieces were flash frozen on dry ice for 5 min and fragmented by centrifugation (6 min, 6,000 rpm) through a hole in a 0.5 mL tube into a 1.5 mL tube.

Protein digest, RNA extraction and sequencing

The eluted RNA-protein complexes were treated with 200 µg Proteinase K in 400 µL Proteinase K buffer (50 mM Tris-HCl pH 7.5, 50 mM NaCl, 0.1 % TritonX-100, 10 mM Imidazole, 1 % SDS, 5 mM EDTA) and 1 µL RNasin RNase inhibitor (Promega). The mix was incubated for 2 h at 55 °C with constant shaking. To extract the RNA an equal volume of Acid-phenol:chloroform (Ambion) was added, and the extracted RNA was precipitated over the weekend. Precipitated RNA was washed with 70 % ethanol, air dried on ice and resuspended in 2.5 µL RNase-free H_2O and 2.5 µL buffer 1 (CleanTag Small RNA library kit). Small RNA libraries were generated using the CleanTag Small RNA library kit (TriLink) following manufacturer's instructions with the following modifications. As the 3' ligation was already complete, library preparation was continued at the 5' adapter ligation step. The adapter was diluted 1:10, libraries were amplified using 20 PCR cycles and a size range of 160-238 bp was

purified from the TBE gel (to avoid the miRNA only band). Samples were then sequenced by Edinburgh Genomics on Illumina NovaSeq using 100 single-end or by Genewiz (Azenta Life Sciences, Germany) using 150 nt paired-end as indicated in Table S1.

Transfection of miRNA mimics/inhibitors, siRNAs and GapmeRs

Synthetic miRNA mimic and inhibitors as well as controls were obtained from Dharmacon, siRNAs were obtained from ThermoFisher and GapmeRs were obtained from Qiagen (see Table S6). A549 cells were reverse transfected using 5 or 10 nM of the respective mimic/inhibitor/siRNA/GapmeRs in 0.3 % Lipofectamine 2000 (Invitrogen). These were pre-incubated with Lipofectamine in Opti-MEM I (Gibco) for 20 min and subsequently added to empty wells of either a 96 well or 6 well plate. The cell mix was added to the transfection mix in antibiotic free DMEM, supplemented with 10 % FBS and 1 % L-Glut. Transfected cells were incubated for 24 h at 37 °C and 5 % CO_2 before cell viability was measured using the CellTiter-Blue reagent (Promega) according to manufacturer's instructions and cells were infected with RSV.

Lentiviral transduction of A549 cells

A549 cells were transduced with lentiviral shMimics (Dharmacon) expressing miR-27a-3p together with turboRFP fluorescent reporter in the pSMART expression system under the human EF1α promoter. Cells were transduced at an MOI of 5 in serum free DMEM (+ 1 % L-Glut) with 8 µg/mL polybrene overnight. The next day FBS-containing media was added to adjust the serum concentration to 10 % and the cells were incubated for another two days. Then the cells were expanded and selected for successful transduction with 1.5 µg/mL puromycin. Serial dilutions of the polyclonal cell populations were used to get single clones and monoclonal cell populations. Clones were assessed for RFP marker expression by microscopy and flow cytometry and miR-27 expression levels by reverse transcription quantitative PCR (see below).

RNA purification and sequencing

Total RNA was extracted from cells using miRNeasy mini kit (Qiagen) according to manufacturer's instructions. If RNA was being used for total RNA-seq, the samples were on-column DNase-treated according to manufacturer's instructions (Qiagen). RNA concentrations were determined using the Qubit RNA HS assay kit (Invitrogen). RNA quality was assessed using Bioanalyzer Pico chips (Agilent).

For total RNA-seq, libraries were prepared by the Genetics Core in Edinburgh using the NEBNext Ultra 2 Directional RNA library prep kit for Illumina and the NEBNext rRNA Depletion kit (Human/Mouse/Rat) according to the provided protocol. Sequencing was performed on the NextSeq 2000 platform (Illumina) using NextSeq 1000/2000 P3 Reagents (200 Cycles) v3. For small RNA-seq, 1 µg of RNA was treated with 5' polyphosphatase (Cambio) according to kit instructions, followed by ethanol precipitation of the RNA. Libraries were generated from 100 ng of RNA using the CleanTag Small RNA library kit (TriLink) according to the manufacture's instruction with the following modifications. Adapters were diluted 1:2, libraries were amplified using 15 PCR cycles and a size range of 147-238 bp was purified from the TBE gel. Libraries were sequenced on the Illumina NovaSeq (Edinburgh Genomics) using 100-base singe end.

Reverse transcription and quantitative PCR

Extracted RNA was reverse transcribed using the QuantiTect RT kit (Qiagen, for total RNA) or miRCURY RT kit (Qiagen, for small RNAs) according to manufacturer's instructions. The resulting cDNA was diluted as per kit instructions and quantified with specific primers

(Table S6) using either QuantiNova SYBR green assays (Qiagen, for cDNA from total RNA) or miRCURY SYBR green assays (Qiagen, for cDNA from small RNAs). Small RNA miRCURY qPCR primer assays were purchased from Qiagen. Primers for the lncRNA PSG were designed to match the lncRNA PSG perfectly but have a mismatch at the 3' end to the parental ZFAND5 gene. Mismatches located in the 3' end were shown to impair PCR amplification (26-28) and allow for differentiation between lncRNA PSG and parental gene. ZFAND5 parental gene primers are located in exon 6 (forward primer) and exon 7 (reverse primer), which according to our data are not expressed at the PSG locus and should only amplify mature mRNA. Data were analysed using the $2^{-\Delta\Delta Ct}$ method (29).

Nuclear fractionation

The nuclear fractionation protocol was adapted from Burke and Sullivan (30). Briefly, cells were harvested and washed with PBS before being lysed in CSKT buffer (10 mM PIPES (pH 6.8), 100 mM NaCl, 300 mM sucrose, 3 mM $MgCl_2$, 1 mM EDTA, 1 mM DTT, 0.5 % Igepal, protease inhibitors (Roche)) on ice for 10 min. Nuclei were pelleted by centrifugation and cytoplasmic fraction (supernatant) was removed. Cytoplasmic fraction was either mixed with an equal amount of SDS lysis buffer (1 % SDS, 2 % β-Mercaptoethanol), boiled at 95°C for 10 min and used for Western blot analysis or RNA was ethanol precipitated for subsequent RNA extraction with the miRNeasy mini kit. Nuclei were washed in CSKT buffer and either lysed directly in SDS lysis buffer for Western blot analysis as described above or Qiazol for RNA extraction. To generate whole cell lysates, harvested cells were directly lysed in SDS lysis buffer/ Qiazol. Equal volumes were maintained for cytoplasmic and nuclear fractions. To test chromatin association of AGO2, the washed nuclei were lysed in CLEAR-CLIP lysis buffer for 20 min. Nuclear soluble fraction (supernatant) was separated from the insoluble fraction (pellet, containing chromatin) by centrifugation. The insoluble fraction was then sonicated 3x 10 s with 30 s on ice in between, followed by treatment with 30 µL DNase RQ1 for 5 min at 37 °C with constant shaking. Equal volumes of extracted RNA were used as input for RT-qPCR. Data were analysed as described in Gagnon et al. (31) with minor modifications. Briefly, data were normalised relative to GAPDH levels in each cellular compartment and the fold change was calculated compared to the whole cell lysate. As miR-27 RT-qPCR was performed with the miRCURY kit that is not designed for mRNA quantification, miR-27 levels were only normalised to the whole cell lysate.

Western blot

Cells were lysed in CLEAR-CLIP lysis buffer or processed as described for nuclear fractionation. Same volumes, equivalent to $1x10^5$ cells were mixed with 4x NuPAGE LDS sample buffer (Invitrogen) and run on a 4-12 % NuPAGE Bis-Tris protein gel in MOPS SDS running buffer (Invitrogen). Proteins were then transferred onto a PVDF membrane (Immobilon-FL, Merck) at 100 V for 105 min. Membranes were blocked with either 3 % milk powder or 5 % BSA in TBS + 0.1 % Tween-20 (TBS-T) and then incubated with the primary antibody overnight at 4 °C. Primary antibodies used in this study: AGO2 (1:1500, clone C34C6, Cell signalling, 2897), α-Tubulin (1:2000, Cusabio, CSB-PA004344), β-Actin (1:1000, Cell signalling, 4967), Calreticulin (1:2000, Cell signalling, 2891), CEACAM1 (1:20,000, Abcam, ab235598), CSF1 (1:1000 in BSA, Abcam, ab9693), Histone H3 (1:2000, Cell signalling, 4499), ZFAND5 (1:1000, Sigma, HPA018129). The next day the membrane was washed with TBS-T and incubated with the secondary antibody (Goat anti-Rabbit IgG (H+L) Secondary Antibody, DyLight 800, Thermo Scientific) diluted 1:20,000 in TBS-T containing 3 % milk or 5 % BSA for 1 h. Membranes were washed again before protein bands were visualised using the Odyssey CLx scanner (Li-cor). For quantification of protein levels, the bands were quantified using Fiji ImageJ (32) as outlined in Stael et al. Section 3.5 (33).

Northern blot

To detect RNAs of interest by Northern blot, 1 µM of the probes (Table S6) were 5' end labelled with [γ^{32}P] ATP (6000 Ci/mmol, Perkin Elmer) using the T4 polynucleotide kinase (10 U/µL, Thermo Scientific) and subsequently cleaned up with Microspin G-25 columns (GE Healthcare) according to the manufacturer's instructions. Equal amounts of extracted RNA (3.5 µg) were mixed 1:1 with Gel Loading Buffer II (Invitrogen) and loaded on a 15% polyacrylamide/8 M Urea gel. RNA Decade Marker (Thermo Scientific) was prepared according to the kit instructions, diluted in Gel Loading Buffer II, and run along the samples. The gel was run in 0.5x TBE at 120 V for 2 h. Samples were then transferred onto a Hybond-N membrane (Amersham Cat. RPN203N, 1 h at 80 V in 0.5x TBE) and chemically crosslinked at 55 °C for 2 h using a solution of 0.16 M EDC (N-(3-Dimethylaminopropyl)-N′-ethylcarbodiimide hydrochloride, Merck) with 0.13 M 1- methylimidazole in H2O (pH 8).(34) The membrane was washed once with 2x SSC (20x SSC, Fisher Scientific) and then pre-hybridised in 4 mL of Perfecthyb Plus hybridisation buffer (Sigma-Aldrich). 5' end labelled probes were heated to 90 °C for 30 s and hybridised to the membrane over night at 42 °C with rotation. The next day the membrane was washed once with the following pre-heated buffers: Wash buffer 1 (2x SSC, 0.1 % SDS), wash buffer 2 (1x SSC, 0.1 % SDS) and wash buffer 3 (0.1x SSC, 0.1 % SDS). To visualise the RNA, the membrane was incubated on a Storage Phosphor screen for 24 h before it was imaged on a Typhoon Scanner (GE Healthcare).

Bioinformatic analysis

Small RNA sequencing analysis

Reads were first quality checked using FastQC (http://www.bioinformatics.babraham.ac.uk/projects/fastqc/) and low quality 3' bases (quality below 20) were removed. The 3' small RNA adapter TGGAATTCTCGGGTGCCA was trimmed using Cutadapt (version 1.15) (35) and only reads containing the adapter and ≥ 18 nt were retained. miRNAs were identified using QuickMIRSeq (36) with standard settings. The QuickMIRSeq output file with miRNA counts was then uploaded on Degust web tool (Version 4.1.3, Powell, 2015, DOI: 10.5281/zenodo.3258933) for differential expression analysis using the Voom/Limma method.

CLEAR-CLIP

Initial processing (quality control and trimming) was performed as described above. For paired-end reads only the forward read was used in the analysis. Non-chimeric miRNA reads were identified by mapping to the mature Human miRNAs (miRbase V22) using bowtie2 (37). All reads were mapped to mature Human miRNAs (miRbase V22) using bowtie2 using local sensitive parameters (--sensitive-local), as this allows for partial alignment of potentially chimeric reads to the miRNA database. If the first part mapped to a miRNA and the remaining part was ≥ 18 nt and mapped to the human genome, this read was classified as miRNA-target-chimera. For the initial round of sequencing (NovaSeq 6000, 100-base, single end - except for 06_Mock (CLEAR_200_UP), see Table S1) we mapped the target part of the read to all human protein coding transcripts (GRCh38.p7, Gencode) using bowtie2. For the final dataset (NovaSeq 6000, 150-base, paired-end, as well as 06_Mock (CLEAR_200_UP), see Table S1), the target part was aligned to the human genome (GRCh38.p7, Gencode) with bowtie2, then the aligned portion is extracted and removed if it matches a low complexity sequence as determined by dustmasker. Those target read portions that were kept were then mapped to the human genome using ShortStack (38) as follows: allowing 1 nt mismatches, requiring reads to have a minimum expression level of 0.5 reads per million (mincov 0.5 rpm), using unique mapping reads as guidance to position multimapping reads (mmap u), disabling

mapping positioning when no unique mapping reads are available as guidance (ranmax 'none'), evaluating all possible sites for multimapping reads (bowtie_m 'all'), merging clusters that are closer than 10 nucleotides apart (pad 10). If a read mapped to multiple locations and/or genome features, nearby unique mapping reads are used to guide the read count distribution of multimapping reads. Genome features included in the analysis were 3' untranslated regions (UTRs), coding sequences (CDS), 5' UTRs, introns, regulatory regions (CTCF binding sites, transcription factor (TF) binding sites, enhancer regions, open chromatin regions, promoter-flanking regions and promoter, unprocessed and processed pseudogenes), tRNAs, lncRNAs, rRNAs and miRNAs. Overlaps between annotations and the chimeric cluster regions were made with bedtools (39). We then applied a set of filters to identify high confidence targets in these interactions. Firstly, target sites needed to be present in ≥ 2 samples of the same condition (RSV-infected or mock-infected). Secondly, as the requirement of only a 1 nt overlap could lead to exceedingly long target sites with little overlap the target site length should be shorter than 150 nt and thirdly the target site must contain a strong miRNA seed site (no-mismatches). The code used for this part of the analysis is available on Zenodo (https://doi.org/10.5281/zenodo.7924850). Chimeric miRNA-RSV interactions were identified as described above, except the target part of the read was required to not map to the human genome and map to the RSV genome (KT992094). miRNA-target binding patterns were predicted using the IntaRNA web tool (40). Raw data as well as a processed table with all miRNA-host target interactions have been deposited on GEO. Accession numbers are listed in the data availability section. Re-analysis of samples from the Moore et al. study (17) was performed by removing degenerate adapters to keep those samples comparable to our data which did not include degenerate adapters.

Total RNA-seq

Read quality and adapter trimming was made with trimmomatic 0.39 (41) using the TruSeq3 PE adapters. Paired-end reads were aligned to the human genome (GRCh38.p7, Gencode) with hisat2 2.2.1 (42). Visualization tracks were made within R with the packages: GenomicAlignments 1.28.0 (43), GenomicRanges 1.44.0, Rsamtools 2.8.0 (DOI:10.18129/B9.bioc.Rsamtools), rtracklayer 1.52.0 (44). Each bam file was read into R with the readGAlignmentPairs function without reading secondary alignments. The strand mode for the GAlignmentPairs object was set to 2. Reads were split by plus or negative strand and coverage was calculated separately; the coverage of the negative strand was multiplied by -1 to show reads below the line. Both coverages were then joined in a single object and saved as bedGraph files, which were subsequently compressed with igvtools 2.5.3 (45) to tdf format.

A custom GFF3 file was built which included gene annotations available through Gencode and regulatory regions provided by Ensembl (release 100), both sources of annotations were merged in R using rtracklayer 1.52.0. All regulatory regions that overlapped any Gencode gene annotations were removed, and the feature type was set to "exon" to allow regulatory regions to be quantified in downstream processes. The number of reads mapping to genomic features were quantified with the featureCounts function implemented in Rsubread (version 2.6.4) R package (46) using the following non-default parameters: isPairedEnd = TRUE, isGTFAnnotationFile = TRUE, fraction=TRUE, largestOverlap=TRUE, strandSpecific = 2.

The upset plot for multiple overlapping annotations was made with the ComplexUpset 1.3.5 R package. Degust web tool (Version 4.1.3, Powell, 2015, DOI: 10.5281/zenodo.3258933) was used for differential expression analysis using the Voom/Limma method, with min gene read count of 4 and min gene CPM of 1 in at least 1 sample. CDF plots were made with ggpubr R package. Target genes with more than one binding site were collapsed to ensure each gene was only present once per category.

Statistical tests

Details regarding the statistical tests used and the represented data can be found in the figure legends, or, for the differential expression analysis in the “Small RNA sequencing”/ “Total RNA-seq” section of the Bioinformatic analysis. Statistical tests were considered significant when P values were less than 0.05. Statistical analyses were performed via GraphPad Prism (Prism Software) or, for the Cumulative Distribution Function (CDF) plots in RStudio using the Wilcox.test function (alternative = “less” ("greater” for inhibitor data)). For the statistic comparison of HC targets vs all targets, HC targets were removed from the “all targets” data set.

RESULTS

CLEAR-CLIP protocol optimisation in A549 cells

To generate a high quality CLEAR-CLIP dataset in A549 cells, we tested and modified several parameters compared to the protocols reported previously (4,17,25). The first step of the protocol involves UV crosslinking to generate covalently linked protein-RNA complexes, where different doses have been used across different cellular contexts (15,17,25,47,48). We found a suitable dose in A549 cells to be 200 mJ/cm^2. In contrast, no crosslinking yielded fewer chimeric reads and was enriched for miRNA reads, as expected from previous literature (17). Higher doses (400 mJ/cm^2) were associated with protein loss and fewer miRNA-target chimeras (Fig S1A-C, Table S1). Irradiated cells were immediately lysed and subsequently treated with RNases and the intermolecular ligation step was carried out with minor modifications (see Materials and Methods). A 3' adapter with an infrared dye allowed for visualisation of the RNA on SDS-PAGE (Fig S1D) and excision of the AGO-RNA complexes was carried out from the gel without the need for transfer to a membrane. We analysed two different molecular weight regions and found the high molecular weight AGO2 enriched for miRNA-target interactions (115-185 kDa, Fig S1C), consistent with previous reports (17,49).

Replicate datasets were generated with A549 cells (1x10^8) either infected with RSV at a multiplicity of infection (MOI) of 0.1 or mock-infected for 48 h (for summary of protocol see Fig 1A). Chimeric reads were identified based on the requirement that the first part of the read maps to a mature miRNA. The remaining part of the read is then used to identify targets with a bioinformatic pipeline that maps reads to the human genome using Shortstack (38) and clusters mapped reads into target sites (Fig 1B, S1G). The percentage of chimeric reads ranged from 3-6 %, on par with previous reports in other cell types (Fig 1C). By mapping to the genome instead of the transcriptome our analysis can identify non-canonical target sites (beyond 3'UTRs or CDS). However, one challenge is the large number of overlapping genome annotations ("Multiple", Fig S1E). Here we classify "multiple" target sites that overlap 3'UTR as 3'UTRs for downstream analysis (> 50 % of the "multiple" target sites overlapped 3'UTRs (Fig S1F)). The remaining target sites with overlapping annotations were kept in the "multiple" category and not further classified (Fig 1D, Fig S1F). The initial analysis of seven datasets (n=3 in Mock and n=4 in RSV-infected) yielded a total of 389,168 and 220,938 unique target sites across Mock and RSV-infected samples, respectively. As a gauge for potential non-specific chimeras that could occur during sample preparation, we note that 10-18 % of the target sites were mapped to ribosomal RNAs (rRNAs, Fig 1D, Table S2); this is comparable to a similar percentage of rRNA chimeric reads in other CLEAR-CLIP reports: 12-17 % in Moore et al. (17) based on re-analysis of their data with our pipeline (Table S2).

Filtering chimeric reads for reproducibility, cluster length and seed sites enriches for miRNA-target interactions in 3' UTRs

Previous studies have shown that AGO scans for targets in a stepwise mechanism, searching first for complementarity with nucleotides 2-4 of the miRNA before extending complementarity to the nucleotides 5-8 (50). To reduce the likelihood of non-specific and non-functional targets in our dataset, we required that chimeras were reproducible in ≥ 2 Mock or ≥ 2 RSV samples, and that the length of the cluster of target reads was < 150 nt (for reference clusters within ribosomal RNAs have a mean of >150 nt whereas those within 3'UTRs are <100 nt; Fig S1G, H). We then applied a further filter to require that target interactions contain canonical seed-based pairing (not allowing mismatches or bulges but allowing 6mer-offset as defined in Bartel (51)) since miRNAs are generally thought to require the interaction with the seed site for efficient inhibition of target translation (51). Our filtering steps of reproducibility, length and seed site resulted in a subset of 7,539 and 2,898 high confidence (HC) target sites in Mock

and RSV-infected samples respectively, with over 50% of the target sites mapping to 3'UTRs (Fig 1E). The HC target sites were enriched for 3'UTRs and CDS (compared to the unfiltered chimeric target list) and all the other target types were depleted, including rRNAs (Fig 1F).

miRNAs miR-26, miR-27 and let-7 interact with specific sites in the RSV genome but are not degraded upon infection

To examine whether RSV interacts directly with host miRNAs, we mapped non-chimeric (AGO binding) and chimeric reads from the CLEAR-CLIP datasets to the RSV genome. Chimeras and AGO binding sites were found across most RSV genes but were by comparison underrepresented in NS1 and L genes (Fig 2A, B). This appears to show selectivity as transcripts for NS1 and L genes are expressed at comparable levels based on RNA sequencing (Fig 2A, top panel). However, 89.1% of RSV-miRNA target sites are neither reproducible nor seed-mediated, suggesting scope for non-specific interactions (Table S1). Strikingly we found that nearly all seed-based chimeras with RSV derive from miR-26-5p, miR-27-3p and let-7-5p. These bind to specific positions in the M, SH, G and NS2 genes (Fig 2C).

Previous studies have shown that interactions with viral RNA can lead to miRNA degradation, in particular in the case of two different herpesviruses targeting miR-27 (5-8) where the viral RNAs exhibit extensive pairing with the 3' end of the miRNA (52). To determine whether miR-27, as well as miR-26 and let-7 were degraded during infection, we examined miRNA expression levels by small RNA-seq. The expression of all three miRNA families is slightly, but not significantly, upregulated in RSV infection at 48 hpi (hours post infection, Fig 2D). In addition, the interactions with RSV do not involve 3' end pairing (Fig S2A-C). However, miR-27 is shortened over the time course of RSV infection from 21 nt to 20 nt - which is not the case for miR-26 or let-7 family members (Fig S2D-F). The effect that this shortening would have on target interaction is not clear, but it has been proposed 3' end variations affect AGO2 binding as well as miRNA-mRNA interactions (53). This could explain the lower percentage of HC chimeras that we observe for miR-27 but not miR-26 or let-7 in RSV infection (Fig 2E).

miR-27 high confidence targets include genes linked to cell cycle regulation and immune signalling

To determine whether the interaction with the viral RNAs could be associated with global de-repression of host miRNA targets upon infection, we compared gene expression in Mock and RSV-infected A549 cells by RNA-seq. We see significant upregulation of miR-26b HC 3'UTR targets and a more subtle de-regulation of miR-26a and miR-27a and miR-27b HC 3'UTR targets whereas there was no de-repression for let-7 targets (Fig S2G-I). Our analysis of RSV, combined with the previous literature in herpesviruses, suggests that miR-27 is directly functionally disrupted by both RNA and DNA viruses and may play important functions in the infection context. Although upregulation of miR-27 targets upon infection was not significant at a global level, we note that many previously validated targets of miR-27 were found to be upregulated upon infection, including WEE1, PLK2 and SPRY2 (Table S3) (54-56).

To probe this further we used the 396 HC 3'UTR targets of miR-27 identified in A549s here to characterize the pathways and networks targeted in human lung cells. GO term analysis using ShinyGO (57) identified several terms related to metabolic processes and cell cycle as enriched among miR-27 targets (Fig 3A), as well as PI3K-Akt and MAPK signalling when investigating KEGG pathways (Fig 3B)(58,59).

To determine whether the HC 3'UTR targets were functionally regulated by miR-27, we overexpressed or inhibited miR-27 using synthetic mimics and inhibitors. Additionally, we generated a lentiviral transduced A549 cell line to stably overexpress miR-27a. Subsequent total RNA-seq showed that overexpression of miR-27 resulted in downregulation of miR-27

HC 3'UTR targets compared to controls (Fig 3C, E). In contrast, miR-27 inhibitors caused a subtle but significant upregulation of miR-27 HC targets (Fig 3D). In all the conditions miR-27 HC 3'UTR targets (395 genes) showed a significantly stronger suppression (and upregulation for the miR-27 inhibitor) compared to analysis of all the miR-27 3'UTR targets for which at least 1 chimera could be found (4415 genes), highlighting the value of our filtering approach to identify functional targets. We observed stronger downregulation using miRNA mimics compared to the miR-27a overexpressing cell line which is most likely due to the difference in miR-27 levels (20-fold overexpression in mimics compared to 3-fold in the cell line; Fig 3F).

The miR-27 mimics significantly reduced the expression of 28 HC 3'UTR target genes associated with cell cycle regulation (Fig 3G, red/purple dots), some of which were also upregulated in RSV infection (labelled dots Fig 3G, Table S3). Although miR-27 has been associated with promotion of cell cycle progression by targeting negative regulators in different cancers (55,60-63) most studies have only focussed on a single target gene. The CLEAR-CLIP data uniquely demonstrates that miR-27 directly regulates many cell cycle-associated genes simultaneously, consistent with its role in promotion of cell cycle (55,60-63). Our high confidence 3'UTR chimeras include previously validated targets such as WEE1, PLK2 and CCNG1 (54,55,64,65), as well as many which have not been associated with miR-27 regulation before, including SGK1, TLK2 and MDM2 (Fig 3G, Table S3). These findings suggest that de-regulation of miR-27 activity by RSV could contribute to cell cycle arrest in infected cells which is known to occur and promote virus replication (66,67).

In addition, miR-27 mimics also caused significant downregulation of target genes associated with PI3K-Akt and MAPK signalling (Fig 3G, blue/purple dots), some of which were also upregulated in RSV infection (Table S3). Interestingly, we found that one of the most strongly downregulated genes in response to miR-27 mimics is *CSF1* (*colony stimulating factor 1*, Fig 3G), a cytokine involved in intercellular signalling and macrophage activation (68). CSF1 protein levels are also slightly reduced in the miR-27a overexpressing cell line (Fig 3H, I) further supporting regulation by miR-27. Our pathway analysis identified additional miR-27 targets associated with "response to cytokine" including Chemokine (C-X-C motif) ligand 2 (*CXCL2*) and *Mitogen-Activated Protein Kinase Kinase Kinase Kinase 3* (*MAP4K3*) (Table S4) which were also significantly downregulated in response to miR-27 mimics (Table S5). Collectively, these data uncover robust targeting of a network of 28 cell cycle genes by miR-27 and suggest a potential role of miR-27 in signalling to immune cells through regulation of genes such as *CSF1* and *CXCL2* which we identify here as targets of miR-27.

Non-canonical targets of AGO2:miR-27 suggest a role in transcriptional gene regulation

Recently, there has been increasing evidence that AGO:miRNAs can also regulate transcription through interaction with promoter-associated lncRNAs, leading to either activation or inhibition of gene expression in the nucleus (69-73). We therefore examined if any classes of regulatory regions were enriched in our HC target sites. Regulatory regions that overlap pseudogenes (PSGs) were found to be the most enriched category in HC chimeras compared to total target datasets (Fig 4A, overlapping PSG). Pseudogene-derived lncRNAs are generally believed to act as miRNA sponges that interfere with regulation of the parental gene by a miRNA (74). However, we hypothesised that some of the interactions might play a role in AGO:miRNA-mediated regulation of gene transcription since many HC PSG target sites overlap transcriptional regulatory regions.

To test this hypothesis, we focused on the top target for miR-27 that overlapped a regulatory region and PSG (top target defined by total read counts and presence in all three Mock samples). This miR-27 target originated from a highly conserved promoter flanking region (reannotated as enhancer in Ensembl release 109) that overlaps *zinc finger, AN1-type domain*

5 (*ZFAND5*) processed PSG on chromosome 19 (Fig 4B). The binding site is located in the CDS of the PSG as well as the parental gene (the PSG does not contain introns or UTRs, Fig S3A). One challenge with studying PSGs is the ability to map reads confidently to either PSG or the parental gene. Nonetheless, some unique mapping reads from RNA-seq confirmed that an RNA is expressed from the PSG locus (Fig 4B), which is further supported by a previous study analysing data from the Genotype-Tissue Expression (GTEx) project (75). According to our data, the PSG is not a full-length transcript but instead a lncRNA which is missing part of exon 5 as well as exon 6 and 7 (Fig 4C, S3A). We will therefore refer to this RNA as PSG lncRNA.

We first examined whether the parental gene *ZFAND5* was regulated by miR-27. The sequences of parental gene and PSG of *ZFAND5* are not identical but have a few single nucleotide variations that enable them to be distinguished by RNA-seq (Fig S3A). Based on the RNA-seq analysis with miR-27 mimics and the A549-miR-27a overexpression cell line, we find no significant miR-27-mediated regulation of *ZFAND5* mRNA (Fig 4D, S3B), which was further confirmed by Western blot of ZFAND5 protein levels (Fig S3D). There was also no effect on the PSG lncRNA by miR-27 manipulation (Fig 4D, S3C). These data suggest that the interaction of miR-27 with the PSG lncRNA does not impact the PSG expression, nor does it impact *ZFAND5* gene expression (the PSG does not appear to act as a “sponge” for the miRNA). Since the PSG overlaps with a regulatory region, we therefore tested if the interaction of miR-27 with the PSG lncRNA could be involved in regulating gene expression of nearby genes. The closest gene was *CEACAM1* (Carcinoembryonic antigen-related cell adhesion molecule 1), an important regulator of immune cell activation (76) which we observe to be up-regulated upon RSV infection (Fig 4B). miR-27 overexpression using the stable cell line (A549 miR-27a) resulted in a reduction in CEACAM1 mRNA and protein levels (Fig 4D-G). The miR-27 mimic showed the same trend, while miR-27 inhibitor slightly increased *CEACAM1* expression (Fig 4E). Our data do not suggest direct regulation of *CEACAM1* by miR-27 because we do not observe HC 3’UTR chimeras with *CEACAM1* RNA. In addition, we note that *CEACAM1* does not have any predicted binding sites for miR-27 in the TargetScan 8.0 database (11). To test if the regulation of *CEACAM1* by miR-27 requires the PSG lncRNA, we inhibited the PSG lncRNA using LNA GapmeRs (Qiagen, Fig 4H). We found that CEACAM1 mRNA and protein levels increased, in parallel with the reduction in PSG lncRNA (Fig 4I-K), similar to the trend we see when miR-27 is knocked down. Knockdown of the PSG lncRNA also partly restored CEACAM1 levels in miR-27a overexpressing cells (Fig S3J). Although the GapmeR also reduces ZFAND5 expression (Fig S3G-I), our data suggest that ZFAND5 itself does not regulate *CEACAM1* since siRNA knockdown of *ZFAND5* did not affect CEACAM1 mRNA or protein levels (or the levels of the PSG lncRNA, Fig 4J, K, S3E, F). These data suggest that both the lncRNA and miR-27 are needed for the suppression of *CEACAM1* expression. Consistent with transcriptional regulation of *CEACAM1* by PSG lncRNA and miR-27:AGO2, we confirmed nuclear localisation of AGO2 and miR-27 as well as nuclear enrichment of PSG lncRNA in A549 cells (compared to ZFAND5 gene, which is not enriched in the nucleus, Fig 5A-C). We also show that a small proportion of AGO2 is associated with the chromatin containing fraction (Nuc insoluble, Fig 5D).

Collectively, these data suggest that lncRNAs derived from regulatory regions can be involved in miRNA-mediated regulation of gene expression in the nucleus and present another function for pseudogenes that relates to the miRNA binding sites encoded within them.

DISCUSSION

Here we adapted CLEAR-CLIP as a powerful method to investigate genome-wide canonical and non-canonical miRNA-target interactions in Mock- and RSV-infected A549 lung epithelial cells. After initial optimisation, we were able to recover a high number of miRNA-target chimeras in both conditions which allowed us to not only investigate the host gene target network of miRNAs in these cells but also interactions with viral RNAs. We show for the first time that RSV directly interacts with three host miRNA families through seed pairing: miR-26, miR-27, and let-7. Previous studies have shown that miR-27 is targeted and degraded by non-coding RNAs from HVS as well as MCMV (5-8) and our results demonstrate that an RNA virus also interacts with this miRNA. This finding suggests a key link between miR-27 and host anti-viral signalling. We use the identification of 396 high confidence targets by CLEAR-CLIP combined with gene expression analysis of miR-27 modulated cells to systematically demonstrate the functionality of targets of miR-27 detected in our study in lung epithelial cells. We show that the inhibition of miR-27 activity by RSV is associated with upregulation of pathways important for RSV infection and replication including PI3K/Akt and MAPK signalling as well as control of cell cycle (67,77-83). In addition, we identify as direct miR-27 targets the cytokine *CSF1* as well as the chemokine *CXCL2* which play important roles in intercellular communication (84).

Notably, miR-27 has a subtle antiviral effect on MCMV (85) as well as different respiratory viruses *in vitro*, including multiple influenza strains, RSV A2 and a more pronounced effect against RSV Bt2a, a recent clinical isolate of RSV (81). Additionally, a previous study in MCMV found that viral mutants unable to degrade miR-27 showed a significant reduction in viral titre in the acute infection in the lung (8). It will be prudent to better understand the role of this miRNA in different respiratory virus infections *in vivo*. Our work suggests that miR-27 target de-regulation not only impacts infected epithelial cells but could affect signalling to immune cells and other cells in the lung environment.

Using our method to select for high confidence target sites, we are uniquely able to address non-canonical targets and show that pseudogenes (PSGs) overlapping regulatory regions are a strong candidate for functional miRNA interactions. We postulate that pseudogenes which contain miRNA binding sites in common with their parent genes can adopt novel functions in the pseudogene, beyond a role as miRNA sponges as previously described (74). We provide evidence that an interaction between miR-27 and a lncRNA derived from a pseudogene can functionally regulate transcription of a nearby gene, *CEACAM1*. We show that both miR-27 and the ZFAND5 PSG lncRNA are required to suppress *CEACAM1* expression. This work brings biochemical evidence for nuclear targets of a miRNA that is sequestered in RSV infection and interfaces with a growing body of literature demonstrating miRNAs and AGOs can operate in the nucleus to silence or activate gene expression (13).

In this study we have focussed on miR-27 targets, however the interaction of RSV with miR-26 and let-7 are also intriguing and merit further attention. miR-26 has been reported to regulate antiviral immunity in several different viral infections (86-89) and has been implicated in the inhibition of TLR4 signalling (90). We demonstrate that RSV has evolved to directly inhibit the functional activity of this miRNA. In contrast to miR-26 regulation, the interaction of RSV with let-7 does not cause global de-regulation of let-7 targets but could be important during the viral life cycle; it is striking that *Pestiviruses* also interact with this miRNA to enhance viral translation and stability (4).

In conclusion, this study provides evidence that pseudogenes are a class of miRNA target that can mediate transcriptional regulation linked to immune signalling and demonstrates a new viral-host interaction in RSV infection. As the field of RNA delivery advances, it will be timely

to test the ability to interfere with virus-mediated miRNA de-regulation in this and other respiratory virus infections. In parallel with new knowledge of non-canonical miRNA targets it will be prudent to understand the extent to which these might contribution to other disease pathologies associated with miRNA or Argonaute de-regulation.

Data Availability

CLEAR-CLIP raw files as well as a processed data table containing all miRNA-host target interactions have been deposited in the Gene Expression Omnibus (GEO) under accession number GSE232686 (https://www.ncbi.nlm.nih.gov/geo/query/acc.cgi?acc=GSE232686). Total RNA-seq of Mock and RSV-infected A549 as well as A549 WT, A549 miR-27a and miR-27 mimics/inhibitors have been deposited in GEO under accession numbers GSE231788 (https://www.ncbi.nlm.nih.gov/geo/query/acc.cgi?acc=GSE231788) and GSE231787 (https://www.ncbi.nlm.nih.gov/geo/query/acc.cgi?acc=GSE231787), respectively. The small RNA-seq data of Mock and RSV-infected A549 has been deposited in GEO under accession number GSE231784 (https://www.ncbi.nlm.nih.gov/geo/query/acc.cgi?acc=GSE231784). The original code used for the CLEAR-CLIP analysis is available at https://doi.org/10.5281/zenodo.7924850

Acknowledgements

The authors thank Dr Alfonso Garrido-Lecca from the Yi group at the University of Boulder for sharing advice on modifications to the CLEAR-CLIP protocol. The authors thank the Macias group from the University of Edinburgh for sharing RT-qPCR primers, as well as the IgG control antibody. The authors also thank Dr Pablo Tristán-Ramos from the Heras group at the University of Granada for discussions around crosslinking conditions during the CLEAR-CLIP protocol optimisation and Dr Anton McCaffrey and Sabrina Shore from Trilink for discussions around the modified 3' adapter. Total RNA-seq library preparation and sequencing was carried out by the Genetics core at the Edinburgh Clinical Research Facility. Small RNA sequencing was carried out by Edinburgh Genomics at the University of Edinburgh.

Author Contributions

S.R. and A.H.B designed the study. All authors participated in the discussion and interpretation of the results. S.R. and J.L. performed the experiments. K.G. optimised the CLEAR-CLIP protocol for the fluorescent 3' adapter. J.W. provided the virus and reagents. S.K. developed the CLEAR-CLIP bioinformatic pipeline in communication with S.R. and C.A.G. J.R.B.B. modified the CLEAR-CLIP pipeline. S.K., J.R.B.B., SR performed the bioinformatic analysis of the (small) RNA-seq data. J.R.B.B and S.R. analysed the data with input from A.H.B and C.A.G. S.R. and A.H.B. wrote the manuscript. All authors revised the manuscript.

Funding:

This work was supported by the Wellcome Trust [RCDF 201083/Z/16/Z and ISSF to A.H.B]; Darwin Trust of Edinburgh to S.R.; and collaborative research funding from Janssen Pharmaceuticals, Inc. (Beerse, BE).

Declaration of Interests

Jin Wu is a paid employee of Janssen Research & Development, Janssen Pharmaceutica NV, Turnhoutseweg 30, 2340, Beerse, Belgium.

REFERENCES

1. Jopling, C.L., Yi, M., Lancaster, A.M., Lemon, S.M. and Sarnow, P. (2005) Modulation of Hepatitis C Virus RNA Abundance by a Liver-Specific MicroRNA. *Science*, **309**, 1577-1581.
2. Shimakami, T., Yamane, D., Jangra, R.K., Kempf, B.J., Spaniel, C., Barton, D.J. and Lemon, S.M. (2012) Stabilization of hepatitis C virus RNA by an Ago2-miR-122 complex. *Proc Natl Acad Sci U S A*, **109**, 941-946.
3. Luna, J.M., Scheel, T.K., Danino, T., Shaw, K.S., Mele, A., Fak, J.J., Nishiuchi, E., Takacs, C.N., Catanese, M.T., de Jong, Y.P. *et al.* (2015) Hepatitis C virus RNA functionally sequesters miR-122. *Cell*, **160**, 1099-1110.
4. Scheel, T.K., Luna, J.M., Liniger, M., Nishiuchi, E., Rozen-Gagnon, K., Shlomai, A., Auray, G., Gerber, M., Fak, J., Keller, I. *et al.* (2016) A Broad RNA Virus Survey Reveals Both miRNA Dependence and Functional Sequestration. *Cell Host Microbe*, **19**, 409-423.
5. Cazalla, D., Yario, T. and Steitz, J.A. (2010) Down-regulation of a host microRNA by a Herpesvirus saimiri noncoding RNA. *Science*, **328**, 1563-1566.
6. Buck, A.H., Perot, J., Chisholm, M.A., Kumar, D.S., Tuddenham, L., Cognat, V., Marcinowski, L., Dolken, L. and Pfeffer, S. (2010) Post-transcriptional regulation of miR-27 in murine cytomegalovirus infection. *RNA*, **16**, 307-315.
7. Libri, V., Helwak, A., Miesen, P., Santhakumar, D., Borger, J.G., Kudla, G., Grey, F., Tollervey, D. and Buck, A.H. (2012) Murine cytomegalovirus encodes a miR-27 inhibitor disguised as a target. *Proc Natl Acad Sci U S A*, **109**, 279-284.
8. Marcinowski, L., Tanguy, M., Krmpotic, A., Radle, B., Lisnic, V.J., Tuddenham, L., Chane-Woon-Ming, B., Ruzsics, Z., Erhard, F., Benkartek, C. *et al.* (2012) Degradation of cellular mir-27 by a novel, highly abundant viral transcript is important for efficient virus replication in vivo. *PLoS Pathog*, **8**, e1002510.
9. Janssen, H.L.A., Reesink, H.W., Lawitz, E.J., Zeuzem, S., Rodriguez-Torres, M., Patel, K., van der Meer, A.J., Patick, A.K., Chen, A., Zhou, Y. *et al.* (2013) Treatment of HCV Infection by Targeting MicroRNA. *New England Journal of Medicine*, **368**, 1685-1694.
10. van der Ree, M.H., de Vree, J.M., Stelma, F., Willemse, S., van der Valk, M., Rietdijk, S., Molenkamp, R., Schinkel, J., van Nuenen, A.C., Beuers, U. *et al.* (2017) Safety, tolerability, and antiviral effect of RG-101 in patients with chronic hepatitis C: a phase 1B, double-blind, randomised controlled trial. *The Lancet*, **389**, 709-717.
11. Agarwal, V., Bell, G.W., Nam, J.W. and Bartel, D.P. (2015) Predicting effective microRNA target sites in mammalian mRNAs. *Elife*, **4**.
12. Chu, Y., Yokota, S., Liu, J., Kilikevicius, A., Johnson, K.C. and Corey, D.R. (2021) Argonaute binding within human nuclear RNA and its impact on alternative splicing. *Rna*, **27**, 991-1003.
13. Stavast, C.J. and Erkeland, S.J. (2019) The Non-Canonical Aspects of MicroRNAs: Many Roads to Gene Regulation. *Cells*, **8**.
14. Dhungel, B., Ramlogan-Steel, C.A. and Steel, J.C. (2018) MicroRNA-Regulated Gene Delivery Systems for Research and Therapeutic Purposes. *Molecules*, **23**, 1500.
15. Helwak, A., Kudla, G., Dudnakova, T. and Tollervey, D. (2013) Mapping the human miRNA interactome by CLASH reveals frequent noncanonical binding. *Cell*, **153**, 654-665.
16. Grosswendt, S., Filipchyk, A., Manzano, M., Klironomos, F., Schilling, M., Herzog, M., Gottwein, E. and Rajewsky, N. (2014) Unambiguous identification of miRNA:target site interactions by different types of ligation reactions. *Mol Cell*, **54**, 1042-1054.
17. Moore, M.J., Scheel, T.K., Luna, J.M., Park, C.Y., Fak, J.J., Nishiuchi, E., Rice, C.M. and Darnell, R.B. (2015) miRNA-target chimeras reveal miRNA 3'-end pairing as a major determinant of Argonaute target specificity. *Nat Commun*, **6**, 8864.
18. Mammas, I.N., Drysdale, S.B., Rath, B., Theodoridou, M., Papaioannou, G., Papatheodoropoulou, A., Koutsounaki, E., Koutsaftiki, C., Kozanidou, E., Achtsidis, V. *et al.* (2020) Update on current views and advances on RSV infection (Review). *Int J Mol Med*, **46**, 509-520.

19. Bakre, A., Mitchell, P., Coleman, J.K., Jones, L.P., Saavedra, G., Teng, M., Tompkins, S.M. and Tripp, R.A. (2012) Respiratory syncytial virus modifies microRNAs regulating host genes that affect virus replication. *J Gen Virol*, **93**, 2346-2356.
20. Thornburg, N.J., Hayward, S.L. and Crowe, J.E., Jr. (2012) Respiratory syncytial virus regulates human microRNAs by using mechanisms involving beta interferon and NF-kappaB. *mBio*, **3**.
21. Bakre, A., Wu, W., Hiscox, J., Spann, K., Teng, M.N. and Tripp, R.A. (2015) Human respiratory syncytial virus non-structural protein NS1 modifies miR-24 expression via transforming growth factor-beta. *J Gen Virol*, **96**, 3179-3191.
22. Bakre, A.A., Harcourt, J.L., Haynes, L.M., Anderson, L.J. and Tripp, R.A. (2017) The Central Conserved Region (CCR) of Respiratory Syncytial Virus (RSV) G Protein Modulates Host miRNA Expression and Alters the Cellular Response to Infection. *Vaccines (Basel)*, **5**.
23. Hallak, L.K., Spillmann, D., Collins, P.L. and Peeples, M.E. (2000) Glycosaminoglycan Sulfation Requirements for Respiratory Syncytial Virus Infection. *Journal of Virology*, **74**, 10508.
24. Guerrero-Plata, A., Casola, A., Suarez, G., Yu, X., Spetch, L., Peeples, M.E. and Garofalo, R.P. (2006) Differential Response of Dendritic Cells to Human Metapneumovirus and Respiratory Syncytial Virus. *American Journal of Respiratory Cell and Molecular Biology*, **34**, 320-329.
25. Bjerke, G.A. and Yi, R. (2020) Integrated analysis of directly captured microRNA targets reveals the impact of microRNAs on mammalian transcriptome. *Rna*, **26**, 306-323.
26. Kwok, S., Kellogg, D.E., McKinney, N., Spasic, D., Goda, L., Levenson, C. and Sninsky, J.J. (1990) Effects of primer-template mismatches on the polymerase chain reaction: Human immunodeficiency virus type 1 model studies. *Nucleic Acids Research*, **18**, 999-1005.
27. Bru, D., Martin-Laurent, F. and Philippot, L. (2008) Quantification of the Detrimental Effect of a Single Primer-Template Mismatch by Real-Time PCR Using the 16S rRNA Gene as an Example. *Applied and Environmental Microbiology*, **74**, 1660-1663.
28. Stadhouders, R., Pas, S.D., Anber, J., Voermans, J., Mes, T.H.M. and Schutten, M. (2010) The Effect of Primer-Template Mismatches on the Detection and Quantification of Nucleic Acids Using the 5' Nuclease Assay. *The Journal of Molecular Diagnostics*, **12**, 109-117.
29. Livak, K.J. and Schmittgen, T.D. (2001) Analysis of relative gene expression data using real-time quantitative PCR and the 2(-Delta Delta C(T)) Method. *Methods*, **25**, 402-408.
30. Burke, J.M. and Sullivan, C.S. (2017) DUSP11 – An RNA phosphatase that regulates host and viral non-coding RNAs in mammalian cells. *RNA Biology*, **14**, 1457-1465.
31. Gagnon, Keith T., Li, L., Chu, Y., Janowski, Bethany A. and Corey, David R. (2014) RNAi Factors Are Present and Active in Human Cell Nuclei. *Cell Reports*, **6**, 211-221.
32. Schindelin, J., Arganda-Carreras, I., Frise, E., Kaynig, V., Longair, M., Pietzsch, T., Preibisch, S., Rueden, C., Saalfeld, S., Schmid, B. *et al.* (2012) Fiji: an open-source platform for biological-image analysis. *Nature Methods*, **9**, 676-682.
33. Stael, S., Miller, L.P., Fernández-Fernández, Á.D. and Van Breusegem, F. (2022) In Klemenčič, M., Stael, S. and Huesgen, P. F. (eds.), *Plant Proteases and Plant Cell Death: Methods and Protocols*. Springer US, New York, NY, pp. 127-137.
34. Pall, G.S. and Hamilton, A.J. (2008) Improved northern blot method for enhanced detection of small RNA. *Nat Protoc*, **3**, 1077-1084.
35. Martin, M. (2011) Cutadapt removes adapter sequences from high-throughput sequencing reads. *2011*, **17**, 3.
36. Zhao, S., Gordon, W., Du, S., Zhang, C., He, W., Xi, L., Mathur, S., Agostino, M., Paradis, T., von Schack, D. *et al.* (2017) QuickMIRSeq: a pipeline for quick and accurate quantification of both known miRNAs and isomiRs by jointly processing multiple samples from microRNA sequencing. *BMC Bioinformatics*, **18**, 180.
37. Langmead, B. and Salzberg, S.L. (2012) Fast gapped-read alignment with Bowtie 2. *Nature Methods*, **9**, 357-359.
38. Axtell, M.J. (2013) ShortStack: comprehensive annotation and quantification of small RNA genes. *RNA*, **19**, 740-751.

39. Quinlan, A.R. and Hall, I.M. (2010) BEDTools: a flexible suite of utilities for comparing genomic features. *Bioinformatics*, **26**, 841-842.
40. Mann, M., Wright, P.R. and Backofen, R. (2017) IntaRNA 2.0: enhanced and customizable prediction of RNA–RNA interactions. *Nucleic Acids Research*, **45**, W435-W439.
41. Bolger, A.M., Lohse, M. and Usadel, B. (2014) Trimmomatic: a flexible trimmer for Illumina sequence data. *Bioinformatics*, **30**, 2114-2120.
42. Kim, D., Paggi, J.M., Park, C., Bennett, C. and Salzberg, S.L. (2019) Graph-based genome alignment and genotyping with HISAT2 and HISAT-genotype. *Nature Biotechnology*, **37**, 907-915.
43. Lawrence, M., Huber, W., Pagès, H., Aboyoun, P., Carlson, M., Gentleman, R., Morgan, M.T. and Carey, V.J. (2013) Software for Computing and Annotating Genomic Ranges. *PLOS Computational Biology*, **9**, e1003118.
44. Lawrence, M., Gentleman, R. and Carey, V. (2009) rtracklayer: an R package for interfacing with genome browsers. *Bioinformatics*, **25**, 1841-1842.
45. Robinson, J.T., Thorvaldsdottir, H., Winckler, W., Guttman, M., Lander, E.S., Getz, G. and Mesirov, J.P. (2011) Integrative genomics viewer. *Nat Biotechnol*, **29**, 24-26.
46. Liao, Y., Smyth, G.K. and Shi, W. (2019) The R package Rsubread is easier, faster, cheaper and better for alignment and quantification of RNA sequencing reads. *Nucleic Acids Research*, **47**, e47-e47.
47. Fu, X., Liu, P., Dimopoulos, G. and Zhu, J. (2020) Dynamic miRNA-mRNA interactions coordinate gene expression in adult Anopheles gambiae. *PLoS Genet*, **16**, e1008765.
48. Stebel, S., Breuer, J. and Rossbach, O. (2022) Studying miRNA-mRNA Interactions: An Optimized CLIP-Protocol for Endogenous Ago2-Protein. *Methods and Protocols*, 10.3390/mps5060096.
49. Chi, S.W., Zang, J.B., Mele, A. and Darnell, R.B. (2009) Argonaute HITS-CLIP decodes microRNA-mRNA interaction maps. *Nature*, **460**, 479-486.
50. Chandradoss, Stanley D., Schirle, Nicole T., Szczepaniak, M., MacRae, Ian J. and Joo, C. (2015) A Dynamic Search Process Underlies MicroRNA Targeting. *Cell*, **162**, 96-107.
51. Bartel, D.P. (2018) Metazoan MicroRNAs. *Cell*, **173**, 20-51.
52. McCaskill, J., Praihirunkit, P., Sharp, P.M. and Buck, A.H. (2015) RNA-mediated degradation of microRNAs: A widespread viral strategy? *RNA Biol*, **12**, 579-585.
53. Tomasello, L., Distefano, R., Nigita, G. and Croce, C.M. (2021) The MicroRNA Family Gets Wider: The IsomiRs Classification and Role. *Frontiers in Cell and Developmental Biology*, **9**.
54. Wuchty, S., Arjona, D., Li, A., Kotliarov, Y., Walling, J., Ahn, S., Zhang, A., Maric, D., Anolik, R., Zenklusen, J.C. *et al.* (2011) Prediction of Associations between microRNAs and Gene Expression in Glioma Biology. *PLOS ONE*, **6**, e14681.
55. Tian, Y., Fu, S., Qiu, G.-B., Xu, Z.-M., Liu, N., Zhang, X.-W., Chen, S., Wang, Y., Sun, K.-L. and Fu, W.-N. (2014) MicroRNA-27a promotes proliferation and suppresses apoptosis by targeting PLK2in laryngeal carcinoma. *BMC Cancer*, **14**, 678.
56. Liu, C., Liang, S., Xiao, S., Lin, Q., Chen, X., Wu, Y. and Fu, J. (2015) MicroRNA-27b inhibits Spry2 expression and promotes cell invasion in glioma U251 cells. *Oncol Lett*, **9**, 1393-1397.
57. Ge, S.X., Jung, D. and Yao, R. (2019) ShinyGO: a graphical gene-set enrichment tool for animals and plants. *Bioinformatics*, **36**, 2628-2629.
58. Kanehisa, M., Furumichi, M., Sato, Y., Ishiguro-Watanabe, M. and Tanabe, M. (2020) KEGG: integrating viruses and cellular organisms. *Nucleic Acids Research*, **49**, D545-D551.
59. Luo, W. and Brouwer, C. (2013) Pathview: an R/Bioconductor package for pathway-based data integration and visualization. *Bioinformatics*, **29**, 1830-1831.
60. Mertens-Talcott, S.U., Chintharlapalli, S., Li, X. and Safe, S. (2007) The Oncogenic microRNA-27a Targets Genes That Regulate Specificity Protein Transcription Factors and the G2-M Checkpoint in MDA-MB-231 Breast Cancer Cells. *Cancer Research*, **67**, 11001-11011.

61. Lerner, M., Lundgren, J., Akhoondi, S., Jahn, A., Ng, H.-F., Moqadam, F.A., Oude Vrielink, J.A.F., Agami, R., Den Boer, M.L., Grandér, D. *et al.* (2011) MiRNA-27a controls FBW7/hCDC4-dependent cyclin E degradation and cell cycle progression. *Cell Cycle*, **10**, 2172-2183.
62. Ye, P., Ke, X., Zang, X., Sun, H., Dong, Z., Lin, J., Wang, L., Liu, W., Miao, G., Tan, Y. *et al.* (2018) Up-regulated MiR-27-3p promotes the G1-S phase transition by targeting inhibitor of growth family member 5 in osteosarcoma. *Biomedicine & Pharmacotherapy*, **101**, 219-227.
63. Su, C., Huang, D.P., Liu, J.W., Liu, W.Y. and Cao, Y.O. (2019) miR-27a-3p regulates proliferation and apoptosis of colon cancer cells by potentially targeting BTG1. *Oncol Lett*, **18**, 2825-2834.
64. Shang, Y., Feng, B., Zhou, L., Ren, G., Zhang, Z., Fan, X., Sun, Y., Luo, G., Liang, J., Wu, K. *et al.* (2015) The miR27b-CCNG1-P53-miR-508-5p axis regulates multidrug resistance of gastric cancer. *Oncotarget*, **7**.
65. Lin, T., Ma, Q., Zhang, Y., Zhang, H., Yan, J. and Gao, C. (2018) MicroRNA-27a functions as an oncogene in human osteosarcoma by targeting CCNG1. *Oncol Lett*, **15**, 1067-1071.
66. Gibbs, J.D., Ornoff, D.M., Igo, H.A., Zeng, J.Y. and Imani, F. (2009) Cell Cycle Arrest by Transforming Growth Factor β1 Enhances Replication of Respiratory Syncytial Virus in Lung Epithelial Cells. *Journal of Virology*, **83**, 12424-12431.
67. Bian, T., Gibbs, J.D., Orvell, C. and Imani, F. (2012) Respiratory syncytial virus matrix protein induces lung epithelial cell cycle arrest through a p53 dependent pathway. *PLoS One*, **7**, e38052.
68. Altan-Bonnet, G. and Mukherjee, R. (2019) Cytokine-mediated communication: a quantitative appraisal of immune complexity. *Nature Reviews Immunology*, **19**, 205-217.
69. Benhamed, M., Herbig, U., Ye, T., Dejean, A. and Bischof, O. (2012) Senescence is an endogenous trigger for microRNA-directed transcriptional gene silencing in human cells. *Nat Cell Biol*, **14**, 266-275.
70. Matsui, M., Chu, Y., Zhang, H., Gagnon, K.T., Shaikh, S., Kuchimanchi, S., Manoharan, M., Corey, D.R. and Janowski, B.A. (2013) Promoter RNA links transcriptional regulation of inflammatory pathway genes. *Nucleic Acids Res*, **41**, 10086-10109.
71. Di Mauro, V., Crasto, S., Colombo, F.S., Di Pasquale, E. and Catalucci, D. (2019) Wnt signalling mediates miR-133a nuclear re-localization for the transcriptional control of Dnmt3b in cardiac cells. *Sci Rep*, **9**, 9320.
72. Turunen, T.A., Roberts, T.C., Laitinen, P., Vaananen, M.A., Korhonen, P., Malm, T., Yla-Herttuala, S. and Turunen, M.P. (2019) Changes in nuclear and cytoplasmic microRNA distribution in response to hypoxic stress. *Sci Rep*, **9**, 10332.
73. Laitinen, P., Väänänen, M.-A., Kolari, I.-L., Mäkinen, P.I., Kaikkonen, M.U., Weinberg, M.S., Morris, K.V., Korhonen, P., Malm, T., Ylä-Herttuala, S. *et al.* (2022) Nuclear microRNA-466c regulates Vegfa expression in response to hypoxia. *PLOS ONE*, **17**, e0265948.
74. Lou, W., Ding, B. and Fu, P. (2020) Pseudogene-Derived lncRNAs and Their miRNA Sponging Mechanism in Human Cancer. *Frontiers in Cell and Developmental Biology*, **8**.
75. Staszak, K. and Makałowska, I. (2021) Cancer, Retrogenes, and Evolution. *Life*, **11**, 72.
76. Gray-Owen, S.D. and Blumberg, R.S. (2006) CEACAM1: contact-dependent control of immunity. *Nature Reviews Immunology*, **6**, 433-446.
77. Pazdrak, K., Olszewska-Pazdrak, B., Liu, T., Takizawa, R., Brasier, A.R., Garofalo, R.P. and Casola, A. (2002) MAPK activation is involved in posttranscriptional regulation of RSV-induced RANTES gene expression. *American Journal of Physiology-Lung Cellular and Molecular Physiology*, **283**, L364-L372.
78. Thomas, K.W., Monick, M.M., Staber, J.M., Yarovinsky, T., Carter, A.B. and Hunninghake, G.W. (2002) Respiratory Syncytial Virus Inhibits Apoptosis and Induces NF-κB Activity through a Phosphatidylinositol 3-Kinase-dependent Pathway*. *Journal of Biological Chemistry*, **277**, 492-501.

79. Gibbs, J.D., Ornoff, D.M., Igo, H.A., Zeng, J.Y. and Imani, F. (2009) Cell cycle arrest by transforming growth factor beta1 enhances replication of respiratory syncytial virus in lung epithelial cells. *J Virol*, **83**, 12424-12431.
80. Krzyzaniak, M.A., Zumstein, M.T., Gerez, J.A., Picotti, P. and Helenius, A. (2013) Host cell entry of respiratory syncytial virus involves macropinocytosis followed by proteolytic activation of the F protein. *PLoS Pathog*, **9**, e1003309.
81. McCaskill, J.L., Ressel, S., Alber, A., Redford, J., Power, U.F., Schwarze, J., Dutia, B.M. and Buck, A.H. (2017) Broad-Spectrum Inhibition of Respiratory Virus Infection by MicroRNA Mimics Targeting p38 MAPK Signaling. *Mol Ther Nucleic Acids*, **7**, 256-266.
82. Preugschas, H.F., Hrincius, E.R., Mewis, C., Tran, G.V.Q., Ludwig, S. and Ehrhardt, C. (2019) Late activation of the Raf/MEK/ERK pathway is required for translocation of the respiratory syncytial virus F protein to the plasma membrane and efficient viral replication. *Cellular Microbiology*, **21**, e12955.
83. Chen, L.-F., Xu, W.-B., Li, Y.-Y., Chen, N.-H., Luo, D., Song, Q.-Y., Tang, W., Huang, Z.-G., Li, Y.-L., Liu, Z. *et al.* (2020) Inhibitory Effect of PIK-24 on Respiratory Syncytial Virus Entry by Blocking Phosphatidylinositol-3 Kinase Signaling. *Antimicrobial Agents and Chemotherapy*, **64**, e00608-00620.
84. Daneshpour, H. and Youk, H. (2019) Modeling cell–cell communication for immune systems across space and time. *Current Opinion in Systems Biology*, **18**, 44-52.
85. Santhakumar, D., Forster, T., Laqtom, N.N., Fragkoudis, R., Dickinson, P., Abreu-Goodger, C., Manakov, S.A., Choudhury, N.R., Griffiths, S.J., Vermeulen, A. *et al.* (2010) Combined agonist-antagonist genome-wide functional screening identifies broadly active antiviral microRNAs. *Proc Natl Acad Sci U S A*, **107**, 13830-13835.
86. Zhao, F., Xu, G., Zhou, Y., Wang, L., Xie, J., Ren, S., Liu, S. and Zhu, Y. (2014) MicroRNA-26b Inhibits Hepatitis B Virus Transcription and Replication by Targeting the Host Factor CHORDC1 Protein*. *Journal of Biological Chemistry*, **289**, 35029-35041.
87. Jia, X., Bi, Y., Li, J., Xie, Q., Yang, H. and Liu, W. (2015) Cellular microRNA miR-26a suppresses replication of porcine reproductive and respiratory syndrome virus by activating innate antiviral immunity. *Sci Rep*, **5**, 10651.
88. Gao, S., Li, J., Song, L., Wu, J. and Huang, W. (2017) Influenza A virus-induced downregulation of miR-26a contributes to reduced IFNalpha/beta production. *Virol Sin*, **32**, 261-270.
89. Zhang, J., Li, Z., Huang, J., Yin, H., Tian, J. and Qu, L. (2020) miR-26a Inhibits Feline Herpesvirus 1 Replication by Targeting SOCS5 and Promoting Type I Interferon Signaling. *Viruses*, **12**, 2.
90. Liu, S., Gao, L., Wang, X. and Xing, Y. (2015) Respiratory syncytial virus infection inhibits TLR4 signaling via up-regulation of miR-26b. *Cell Biol Int*, **39**, 1376-1383.

Figure 1

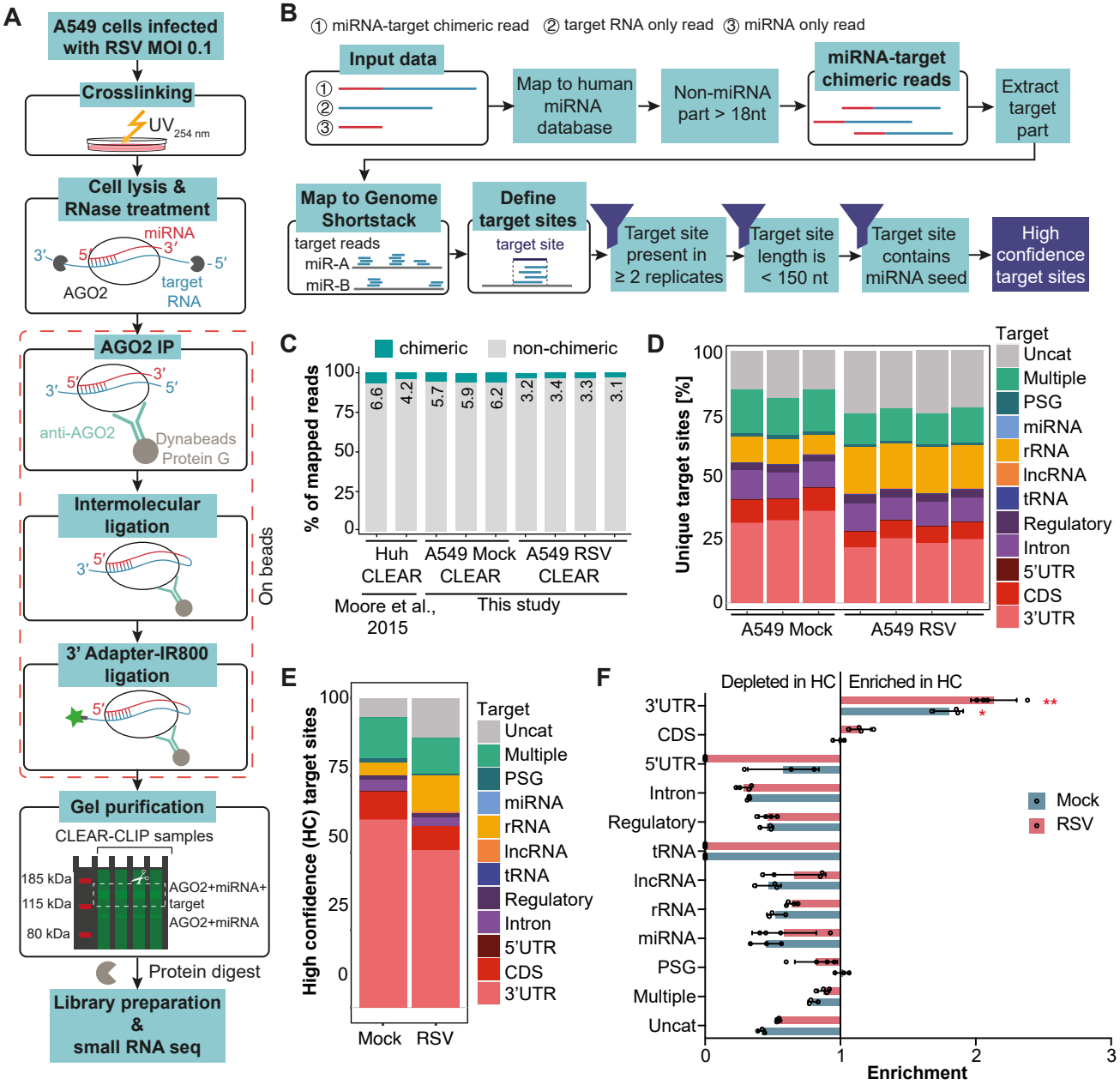

miRNA target sites in RSV-infected A549 cells discovered by CLEAR-CLIP.(**A**) Overview of CLEAR-CLIP protocol. (**B**) Schematic of bioinformatics pipeline: chimeric reads were defined as the first part of the read mapping to a mature miRNA with the remaining part ≥ 18 nt. Target sites were extracted and mapped to the human genome and subsequently clustered into target sites per miRNA. To remove background of non-specific interaction, target sites were filtered for reproducibility, length <150nt and presence of the miRNA seed. (**C**) Percentage of chimeric vs non-chimeric reads mapping to the human genome in our samples (three biological replicates for Mock and four for RSV) compared to the Moore et al. study(17). (**D**) Percentage of unique target sites across different RNA categories. Target regions are 3' untranslated region (3'UTR), coding sequence (CDS), 5'UTR, introns, regulatory regions (Regulatory), transfer RNA (tRNA), long noncoding RNA (lncRNA), ribosomal RNA (rRNA), miRNA, pseudogenes (PSG), multiple annotations (Multiple) or uncategorised (Uncat). (**E**) Percentage of unique high confidence (HC) target sites across different RNA categories described in D). (**F**) Enrichment of HC target sites compared to non-filtered target sites. Red asterisks indicate significant enrichment (One Brown-Forsythe and Welch ANOVA with Dunnett's T3 multiple comparisons test performed separately for Mock and RSV samples, * P ≤ 0.05, ** P ≤ 0.01).

Figure 2

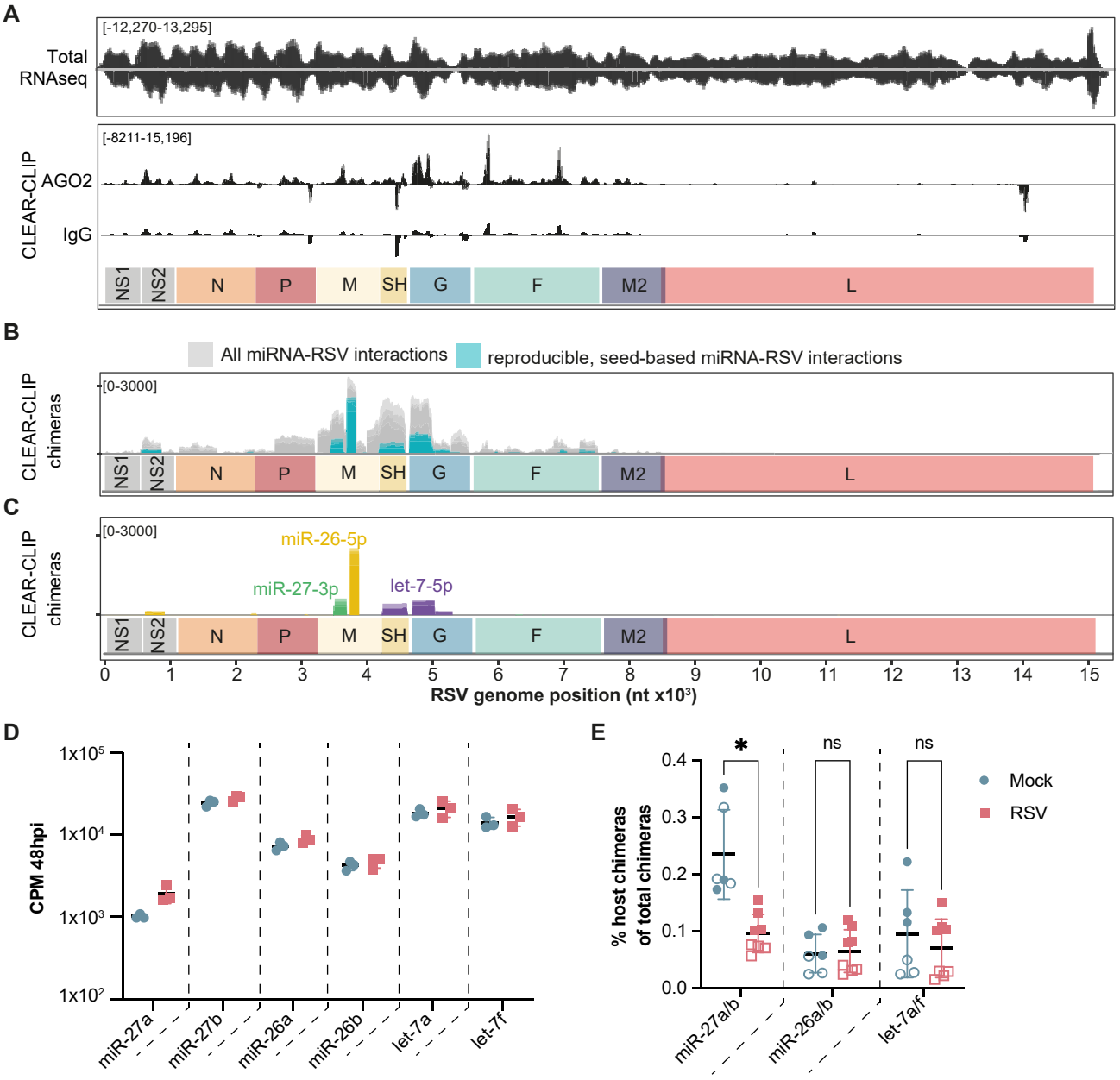

miRNA interactions with the RSV genome do not lead to miRNA degradation but affect target interactions. (**A-C**) Genome browser view of the RSV genome (KT992094) showing total RNA-seq read coverage (top panel), as well as AGO2 and IgG binding (determined from non-chimeric reads mapping to RSV, lower panel) (**A**), all miRNA chimeras (grey) and seed-based, reproducible miRNA chimeras (blue) (**B**), and reproducible, seed-based binding sites for miR-26 (yellow), miR-27 (green), and let-7 (purple) (**C**). (**D**) miRNA expression determined by small RNA-seq in counts per million (CPM) at 48 hours post infection (hpi) in Mock vs RSV-infected cells for miR-27a/b, miR-26a/b and let-7a/f. Shown are three biological replicates with mean. Significance was tested using multiple unpaired t-tests for each miRNA family member: all changes between Mock and RSV are non-significant. (**E**) Percentage of host HC miRNA-target site reads of total chimeric reads in Mock vs RSV-infected samples for miR-27a/b, miR-26a/b and let-7a/f. Significance was tested using multiple unpaired t-tests (ns = non-significant, * $P \leq 0.05$). Different miRNA family members are highlighted by filled (miR-27a, miR-26a, let-7a) or open symbols (miR-27b, miR-26b, let-7f).

Figure 3

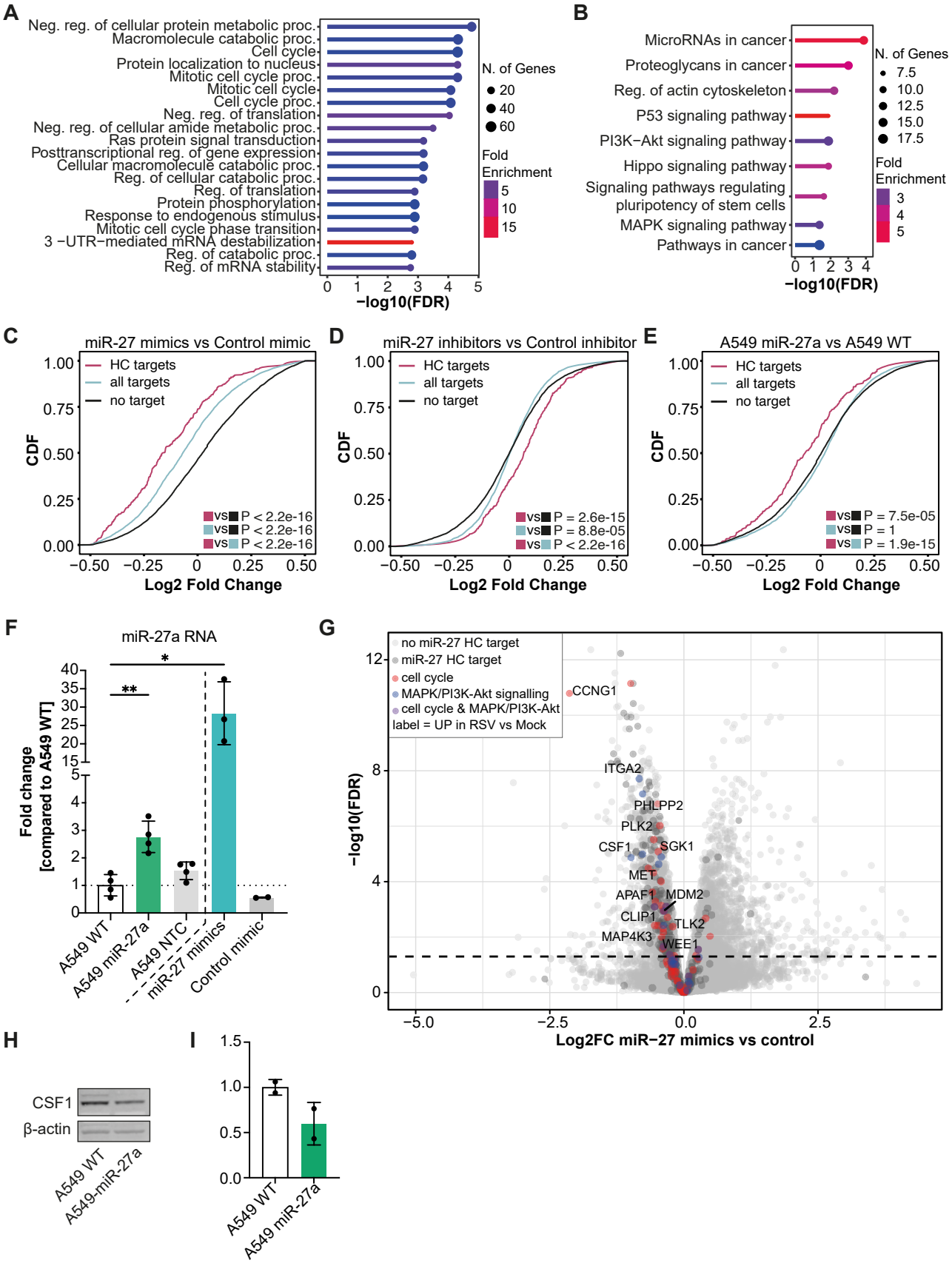

miR-27 regulates genes associated with cell cycle progression and immune signalling. (**A,B**) Pathway analysis of miR-27 HC 3'UTR target genes using ShinyGO V0.77 (57) showing significant pathways (limited to 20 pathways, FDR < 0.05, pathway size: min. 2, max. 2000) for GO term Biological process (**A**) and KEGG pathways (58,59) (**B**). (**C-E**) Cumulative distribution function (CDF) plot of RNA-seq data comparing the log2 fold change of miR-27 HC 3'UTR target genes (red) vs all miR-27 3'UTR target genes (blue) and no target genes (black) between A549 cells transfected with 10 nM miR-27 mimics or control mimic (**C**), miR-27 inhibitor and control inhibitor transfected cells (**D**) and lentiviral transduced cell line stably overexpressing miR-27a (A549 miR-27a) and A549 wildtype (A549 WT) cells (**E**). (**F**) qPCR results of fold change in miR-27 levels in A549 WT, A549 miR-27a, A549 transduced with a non-targeting control (A549 NTC), miR-27 mimic transfected and control mimic transfected cells. Shown are biological replicates with mean ± SD. Significance was tested using One-way ANOVA with Welch's correction (* P ≤ 0.05, ** P ≤ 0.01). (**G**) Volcano plot of RNA-seq data showing log2 fold change (Log2FC) in gene expression in miR-27 mimic transfected cells compared to mimic control transfected cells. Highlighted are: miR-27 HC targets (dark grey), miR-27 HC targets associated with cell cycle (red) or MAPK/PI3K-Akt signalling (blue). Purple dots highlight HC targets belonging to both pathway categories. Gene names are shown for genes that were upregulated (log2 fold change > 0) in the RNA-seq data of RSV vs Mock-infected cells. (**H**) Western blot analysis of CSF1 protein expression in A549 WT or miR-27a overexpressing cells at 48hpi compared to β-Actin loading control. (**I**) Quantification of CSF1 protein levels from H) normalised to β-Actin, shown as mean ± SD for two biological replicates.

Figure 4

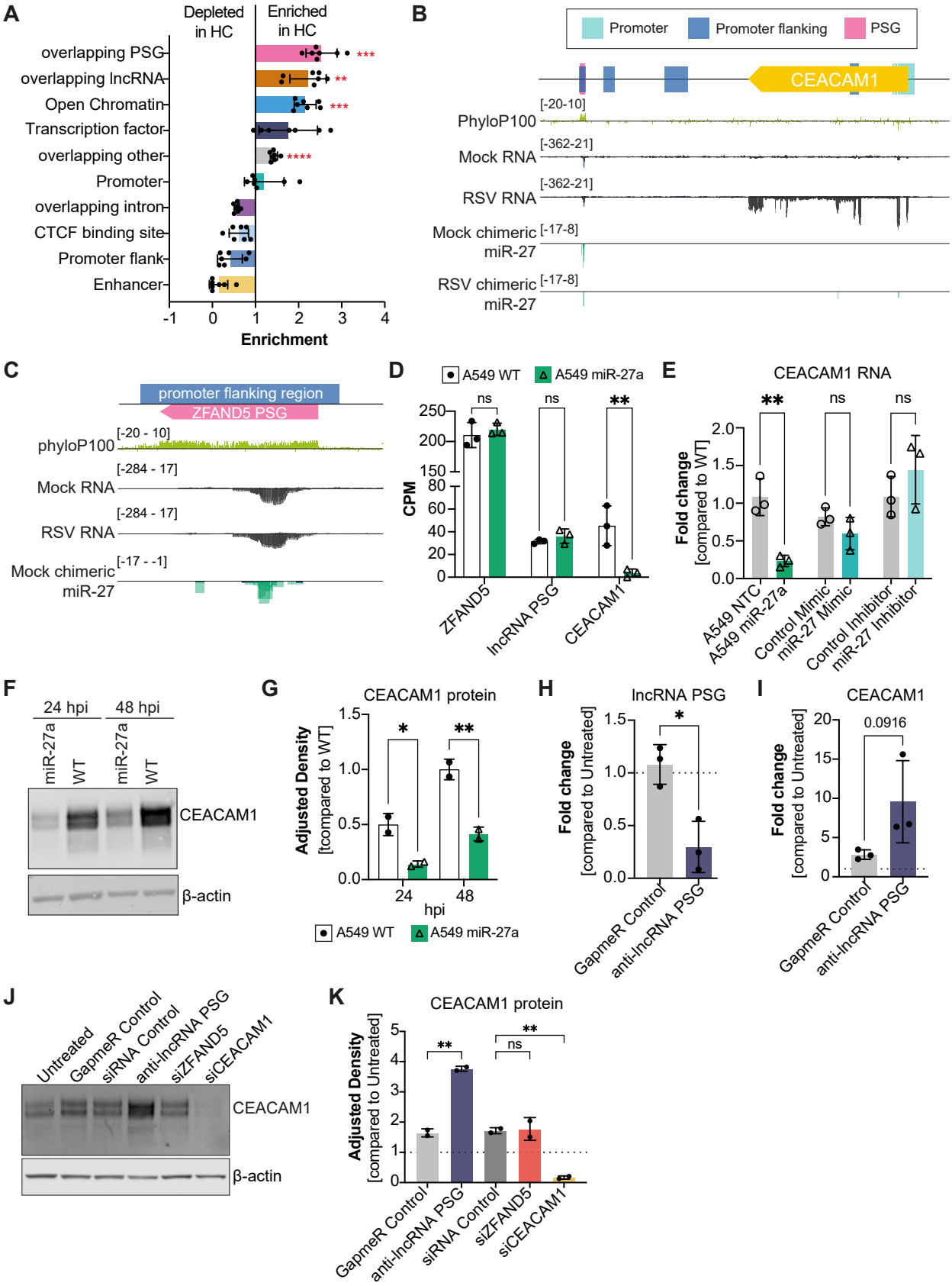

Non-canonical targets of Ago2:miR-27 suggest a role in transcriptional regulation of CEACAM1. (**A**) Enrichment of HC target sites in regulatory regions compared to non-filtered target sites. Target sites were filtered to remove target sites from 3'UTRs and CDS. Shown are mean SD for three Mock and four RSV CLEAR-CLIP replicates combined. Red asterisks indicate significant enrichment (One Brown-Forsythe and Welch ANOVA with Dunnett's T3 multiple comparisons test. Due to the low number of target sites in some of the categories, Mock and RSV samples were analysed together for more statistical power, * P ≤ 0.05, ** P ≤ 0.01, *** P ≤ 0.001, **** P ≤ 0.0001). "Overlapping" indicates regulatory regions overlapping other genome annotations (pseudogenes (PSG), lncRNAs and introns). (**B,C**) Genome browser view of the genomic location of top miR-27 regulatory target overlapping a PSG, showing the conservation using PhyloP100, features of the genomic locus, total RNA-seq coverage in Mock and RSV-infected samples (n = 3), as well as miR-27 target site coverage (chimeric miR-27) in Mock and RSV-infected CLEAR-CLIP samples for miR-27 binding site and nearby genome features (**B**) or a zoom into the promoter flanking/PSG region (**C**). (**D**) RNA-seq data comparing gene/lncRNA expression in CPM in A549 WT cells and A549 cells overexpressing miR-27a (A549 miR-27a). Shown are three biological replicates with mean SD. Significance was tested with two-way ANOVA with Sidak's multiple comparisons test (ns = non-significant, ** P ≤ 0.01). (**E**) qPCR results of fold change in CEACAM1 mRNA expression in response to miR-27 overexpression (A549 miR-27a, miR-27 Mimic) or inhibition (miR-27 Inhibitor) and controls (A549 NTC, Control Mimic, Control Inhibitor). Mimics/ inhibitors were transfected at a final concentration of 10 nM. Data is shown as mean ± SD. Significance was tested with two-way ANOVA with Sidak's multiple comparisons test (ns = non-significant, ** P ≤ 0.01).

continued on next page

Figure 4 continued

(**F**) Western blot analysis of CEACAM1 protein at 24 hpi and 48 hpi (RSV MOI 0.1) in response to miR-27a overexpression compared to β-Actin loading control. (**G**) Quantification of CEACAM1 protein levels from F) corrected for β-Actin and normalised to A549 WT. Shown are two biological replicates with mean ± SD. Significance was tested with two-way ANOVA with Sidak's multiple comparisons test (*P ≤ 0.05, ** P ≤ 0.01). (**H,I**) qPCR results of lncRNA PSG expression (**H**) or CEACAM1 expression (**I**) after treatment with 5 nM GapmeR targeting lncRNA PSG (anti-lncRNA PSG) or control. Shown are two biological replicates with mean ± SD. Significance was tested with unpaired two-tailed t-test (ns = non-significant, * P ≤ 0.05). (**J**) Western blot analysis of CEACAM1 after treatment with anti-lncRNA PSG GapmeR, siRNAs against ZFAND5 (siZFAND5) and CEACAM1 (siCEACAM1) and controls in comparison to β-Actin loading control. (**K**) Quantification of CEACAM1 protein levels from J) corrected for β-Actin and normalised to Untreated control. Shown are two biological replicates with mean ± SD. Significance was tested with One Brown-Forsythe and Welch ANOVA with Dunnett's T3 multiple comparisons test.

Figure 5

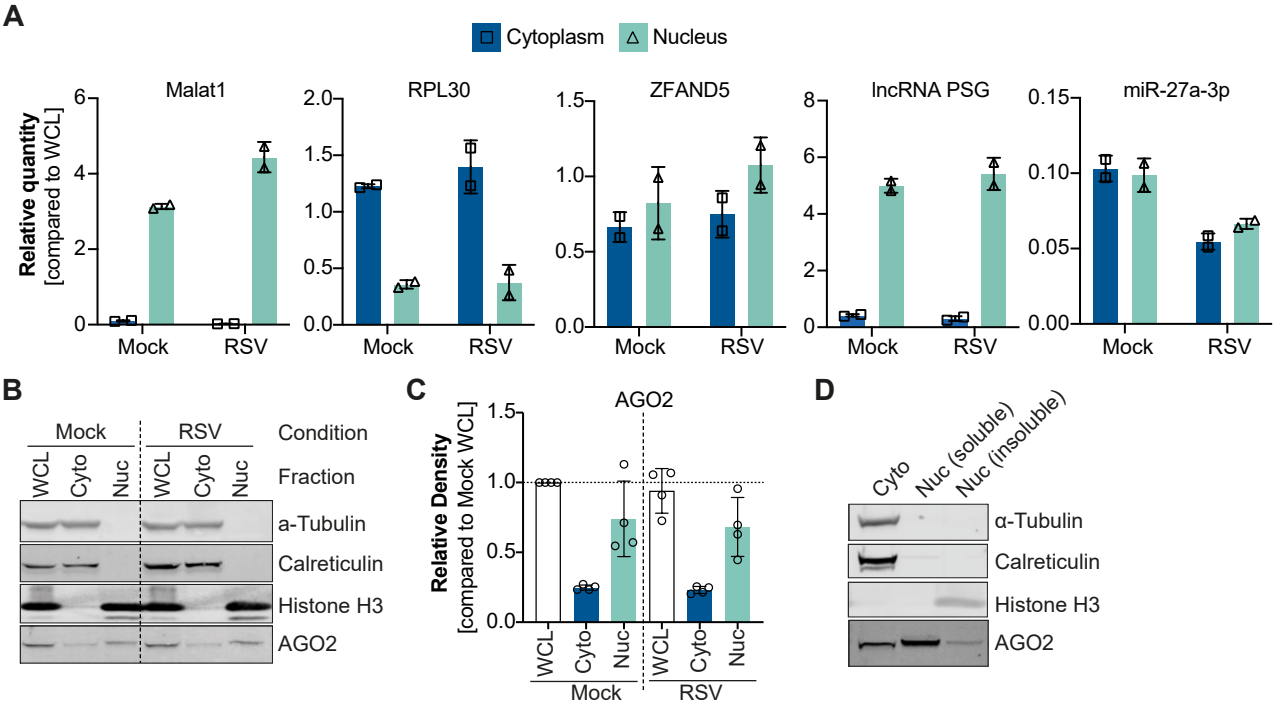

AGO2, miR-27 as well as the lncRNA PSG are present in the nucleus of A549 cells. (**A**) qPCR results for Malat1, RPL30, ZFAND5, PSG lncRNA and miR-27 (left to right) levels in cytoplasmic and nuclear fractions in Mock and RSV-infected cells. Data is shown as mean ± SD for two biological replicates. (**B**) Western blot analysis of AGO2 protein levels in subcellular fractions showing whole cell lysate (WCL), cytoplasmic (Cyto), as well as nuclear (Nuc) fractions for Mock and RSV-infected cells. α-Tubulin and Calreticulin were used as cytoplasmic markers and Histone H3 as nuclear marker. (**C**) Quantification of AGO2 protein levels in B). Data is shown as mean ± SD for four biological replicates and normalised to WCL Mock. (**D**) Western blot analysis of cellular fractionation showing cytoplasmic fraction (Cyto), as well as the soluble and insoluble nuclear fractions (Nuc). α-Tubulin and Calreticulin were used as cytoplasmic markers and Histone H3 as nuclear marker associated with the chromatin.